Noname manuscript No.
(will be inserted by the editor)

Global linear instability of flow through a converging-diverging channel

Gayathri Swaminathan · Mamta R. Jotkar · Kirti Chandra Sahu · Rama Govindarajan

Received: date / Accepted: date

Abstract The global linear stability, where we assume no homogeneity in either of the spatial directions, of two-dimensional laminar base flow through a spatially periodic converging-diverging channel is studied at low Reynolds numbers. A large converging-diverging angle is used, to achieve critical Reynolds numbers of the first instability of below 10. These values are significantly lower than those reported earlier at smaller amplitudes of wall waviness. The leading disturbance mode is seen to be a stationary mode. The eigenspectrum has a branched structure, with modes on the upper branch displaying a variety of structures. Our global stability study suggests that such modes can be tailored to give enhanced mixing in micro channels at low Reynolds numbers.

1 Introduction

The study of flow through spatially varying geometries has received considerable attention in the recent past, both numerically and experimentally (see e.g [1–3]) due to its relevance in various microfluidic applications. Many researchers, e.g. [4] have conducted direct numerical simulations and experiments in order to understand the phenomenon of mixing, which has been an issue in microfluidic devices ranging from microscale reactor to the biological flows [5]. If the steady laminar flow were to be unstable to linear perturbations, it might help one to enhance mixing levels. In general, however, flow in these small scale geometries, with the associated very low flow rates, tends to be stable to perturbations. One of the ways of achieving low Reynolds number instabilities is to introduce convergences and divergences [6–14] in the flow channel. A global linear stability analysis of such geometries will help determine how small the Reynolds number can be where a first instability arises. In this paper, we investigate the flow instability in a periodic converging-diverging channel by conducting a global stability analysis, and also by obtaining two-dimensional nonlinear periodic solutions. Our work is conducted at Reynolds numbers significantly lower than is usual for such global stability studies.

Laminar flow through straight pipes and channels exhibits subcritical algebraic growth of disturbances, and transition to turbulence takes place at a Reynolds number where the flow is predicted by a modal analysis to be linearly stable. On the other hand, if the pipe or channel is not straight but contains regions of wall divergence, one can have exponential growth of small disturbances at low Reynolds numbers. Laminar flow through a two-dimensional straight channel is linearly unstable at Reynolds number higher than 5772.2 (based on channel half-width and centerline velocity), but a wall-divergence of less than a degree brings down the critical Reynolds number, Re_{cr} (be-

G. Swaminathan
Airbus Engineering Centre India Pvt. Ltd., Bangalore - 560016, India

M. Jotkar
Tata Institute of Fundamental Research, Centre for Interdisciplinary Sciences, Hyderabad - 500075, India
E-mail: mamtaj@tifrh.res.in

K. C. Sahu
Department of Chemical Engineering, Indian Institute of Technology Hyderabad, Yeddumailaram 502 205, Telangana, India

R. Govindarajan
Tata Institute of Fundamental Research, Centre for Interdisciplinary Sciences, Hyderabad - 500075, India

low which the flow is linearly stable) by an order of magnitude. This was shown by Eagles [15] a long time ago. In a circular pipe the effect of the angle of divergence is even greater, as the critical Reynolds number decreases all the way from infinity, for a straight pipe, to the order of 100, for a diverging pipe having an angle of divergence of 3° [16]. Conversely, a contraction or convergence stabilizes the flow very strongly, see e.g. Alpine et al. [1]. All these early studies assumed that the basic flow is either fully-developed or self-similar, and analysed the behaviour of a infinitesimally small disturbance. However, this assumption does not hold good in the geometries of our concern, particularly at low Reynolds number. Recently Swaminathan et al. [2] studied the stability characteristics of flow through a diverging channel by conducting a global stability analysis.

Consider now a wavy-walled channel of constant average width, with alternating diverging and converging sections. The first question that would arise here is whether the destabilising effect of divergence is cancelled by the subsequent convergence. The answer is no: the stability of flow through such a geometry has been studied well and the conclusion that emerges is that this flow is linearly unstable at a far lower Reynolds number than in a straight channel [17]. Due to this fortunate circumstance, a converging-diverging geometry becomes a good configuration for achieving mixing at low Reynolds numbers and finds application in small scale flows.

A typical periodic unit of a sinusoidal channel (symmetric about the axis shown as vertical in the figure) studied in this work is shown in figure 1. The amplitude of wall waviness is measured by a parameter ϵ, defined here as the ratio of the maximum difference in widths to the minimum width. We define our 'standard' geometry as the one with $\epsilon = 2.3$ and domain length $L = 10$. The parameter ϵ is varied to study the effect of wall-waviness of the flow stability.

Many converging-diverging geometries have been studied before, and available values for the critical Reynolds number Re_{cr}, below which flow is linearly stable in the modal sense to all small perturbations, are compiled in figure 2 as a function of the wall waviness amplitude ϵ. A consistent trend is visible, where the Re_{cr} decreases with increase in the waviness amplitude, although the geometries included differ quite significantly. The aspect ratio, i.e. the length of a given periodic unit as compared to the average width of the channel, ranges from about 0.6 to 600 in the results shown. Wall shapes also differ, some are sinusoidal, triangular grooved, arc-shaped etc. Also the experiments of Stephanoff et al. [7] on various types of periodic

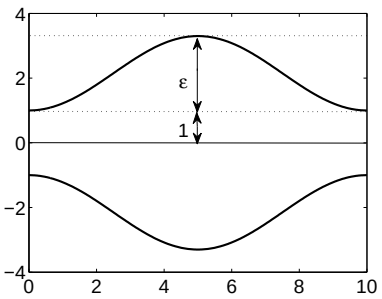

(a)

Fig. 1 Schematic of a symmetric sinusoidal channel under study. Ratio of the amplitude of the wall waviness and to the minimum width of the channel, $\epsilon = 2.3$ and domain length is fixed at $L = 10$. Note that in a typical microchannel, several geometries like this one will be connected in series.

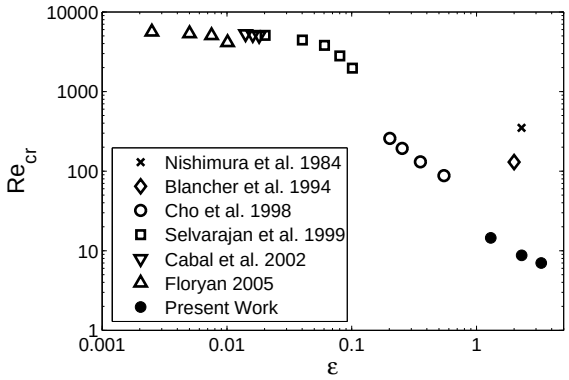

Fig. 2 Variation of the critical Reynolds number Re_{cr} with the wall waviness amplitude ϵ in selected previous studies. Although different studies have used different aspect ratios, different domain length and different wall shapes, a trend is observed. Note that the result of Nishimura et al.[8] shown here does not correspond to the critical Reynolds number. The study of Blancher et al [9] is on a different geometry. Please see text for further details.

grooved channels such as the sinusoidal, arc-shaped and triangular grooved channels show that the critical Reynolds number depends only on the amplitude rather than the shape of the grooves. It is evident that ϵ is the most important parameter governing the critical Reynolds.

While we have not yet described our approach, we wish to kindle the reader's interest by presenting the results for critical Reynolds number at three different divergence ratios in the same figure (figure 2). It is seen that the trend observed at low ϵ by others is continued to high ϵ, with the appealing consequence that we are able to achieve flows which are unstable at a critical Reynolds number which is an order of magnitude lower than in earlier studies. Two data points of

earlier work at high ϵ seem at first sight to be outliers on this graph. However, the geometry of [9] is very different from the present one, in that it is not a varicose (top-down symmetric) channel. Given that the entire qualitative nature of the mean flow is different, a large difference in the critical Reynolds number is not surprising. We find that the primary bifurcation in this range is always caused by a standing wave. On the other hand, Blancher et al.'s geometry exhibits an onset of instability in the form of a travelling wave. Nishimura et al. [8] do not conduct a stability analysis. They conduct an experiment where they notice full blown turbulence at a Reynolds number of 350. Unsteady laminar flow could exist below this Reynolds number.

In general a channel will consist of several diverging-converging units connected in series. We assume here a flow that is repeating itself from one unit to the next, i.e. periodicity is imposed at the inlet and the outlet. Future studies without thisx assumption are warranted. Note that the assumption leads to completely valid disturbance eigenmodes, but these are only a subset of all possible linear modes. So releasing this assumption will only bring down the critical Reynolds number further. We will find that even when the separation between maxima in disturbance amplitudes is small compared to the length of a periodic unit, disturbance eigenfunctions are usually not wave-like, in that downstream behavior may vary from one normal location to another.

In our discussion of earlier work, we do not dwell on the huge body of work on extremely small ϵ corresponding to wall roughness. We also restrict our attention to periodic geometries with top-down symmetry, i.e., to varicose channels. Stone and Vanka [13] studied the flow numerically through 14 geometric units by imposing convective type of boundary condition at the outlet; whereas Blancher et al. [18] demonstrated self-sustained oscillations without asumming periodicity within a geometric unit. The results of the latter were consistent with the experiments conducted by Kim [19] and Rush et al. [11]. Guzman et al.[20], in numerical simulations, found supercritical Hopf bifurcations before a chaotic flow regime was reached. A large reduction in Re_{cr} with wall waviness was demonstrated [8,10]. In the limit of ϵ tending to zero, traveling Tollmien-Schlichting waves are the most unstable. Beyond a critical waviness amplitude of $\epsilon \sim 0.1$, instability is dominated by three-dimensional oscillatory modes, especially streamwise vortices, which are driven by centrifugal effects induced by the concavity of the wall [21,10,14]. As ϵ is increased further, beyond $\epsilon \sim 0.3$, two-dimensional traveling waves are the most dominant again. The appealing and computationally efficient approach of Floryan [14] and Floryan [22] comes closest to a global stability study. Critical conditions in three dimensions, or the occurrence of both traveling wave instability and vortex instability have been obtained, and detailed studies on the shape, spacing etc. of roughness elements have been carried out [23–25]. Szumbarski and Floryan[26] studied the transient growth associated with channels with wall corrugations and calculated the maximum growth and optimal perturbations for different corrugations. Laval et al.[27] have carried out direct numerical simulations for adverse-pressure gradient flows in the converging-diverging channels. Some experimental analyses on microchannels with complex geometries include Akbari et al.[28] and Duryodhan et al.[4]. The latter experiments analysed the effect of diverging microchannels on flow behavior in order to design effective diffusers. Jose and Cubaud[29] studied immiscible fluids forming drops and its coalescence in a channel with a converging-diverging type of geometry. Peixinho et al. [30, ?] carried out experiments confirming the linear stability results of [16] in a slowly diverging pipe. It was also observed that at low Reynolds number a separated flow appears which increases with increasing Re and further becomes unsteady, leading ultimately to turbulent flow.

These exciting solutions indicate interesting possibilities in the nonlinear regime for the present geometry. Some interesting work in the transition to chaos in such converging-diverging channels include Guman et al. [20], Amon et al. [31].

In a parallel flow, two-dimensional perturbations would be the most unstable, in accordance with Squire's theorem [32]. This theorem is not valid for a non-parallel flow, but going by Cho et al.[10] which shows that two-dimensional disturbances are dominant beyond $\epsilon = 0.3$, we restrict ourselves to two-dimensional disturbances. Three-dimensional disturbances may well prove to be faster growing, both exponentially and algebraically, but the proof of principle is already achieved with two-dimensional disturbances.

The rest of the paper is organised as follows: Section 2 presents the formulation of the problem and the geometry studied here. The computation of the two-dimensional steady base flow is discussed in 2.1 and the global linear stability analysis is explained in 2.2. Section 3 shows the results obtained and section 4 consists of a brief discussion and summary.

2 Problem Formulation

Consider a converging-diverging channel formed by a simple sine function defined appropriately, such as the one shown in the figure 1. The flow is from left to right. The minimum half-width is fixed to 1 while the parameter, ϵ, defined as the ratio of the maximum amplitude of wall-waviness to the minimum half-width, is varied from 0.05 to 3.3 in this work. Unless otherwise specified, the domain length of each repeating unit of the channel is $L = 10$, which is 5 times the minimum width of the channel.

2.1 Base Flow

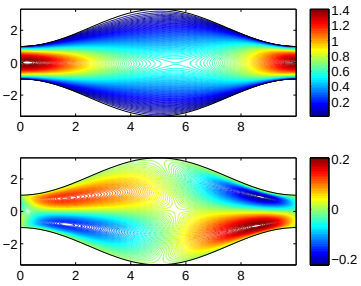

Fig. 3 Contours of streamwise, U (top) and transverse, V (bottom) velocities of the base flow obtained from numerical simulations, for a symmetric case with $\epsilon = 2.3$ and $L = 10$ as shown in the parameter setting explained in the figure 1, at a Reynolds number of 5.

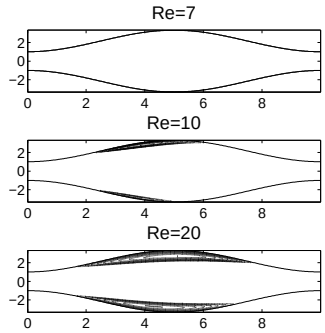

Fig. 4 Contours of streamwise velocity component, U for a symmetric case with $\epsilon = 2.3$ and $L = 10$ and the corresponding laminar separation bubble formation for different Re as shown in the figure. The shaded region shows the separation bubble formed at the walls, containing recirculating flow. Notice that the bubbles at $Re = 20$ at the top and bottom walls differ slightly.

The steady two-dimensional Navier-Stokes equations are solved in the streamfunction-vorticity formulation (obtained after eliminating pressure). This can become very time consuming, so a full multigrid technique is used to accelerate the convergence. This solver has been used in a variety of flows, see e.g. [16],[33]. The code has been validated against several analytical solutions and in several known geometries. The agreement in each case is very good. The governing dimensionless equations are,

$$\frac{\partial \Omega}{\partial t} + (\mathbf{U}.\nabla)\Omega = \frac{1}{Re}\nabla^2\Omega, \tag{1}$$

$$\Omega = -\nabla^2\psi, \tag{2}$$

$$(U, V) = \left(\frac{\partial \psi}{\partial y}, -\frac{\partial \psi}{\partial x}\right), \tag{3}$$

where $\mathbf{U}(U, V)$ is the velocity vector, wherein U and V are the velocity components in the streamwise and transverse directions, respectively; t is time; Ω and ψ are the mean vorticity and streamfunction, respectively, and $\nabla^2 = \partial^2/\partial x^2 + \partial^2/\partial y^2$. The Reynolds number Re is based on the minimum half-width of the channel, and the centerline velocity at the minimum half-width. In order to handle the curved walls, the above equations are solved in the computational domain (ζ, η), which is obtained by the following coordinate transformation:

$$\zeta = x, \quad \eta = y/H(x), \tag{4}$$

subject to the no-slip and impermeability boundary conditions, $U = V = 0$, at the walls; and periodic boundary conditions at the inlet and the exit. In the transformed coordinate, the channel walls are straight and located at $y = \pm 1$. The resultant solution is then transformed back to the physical domain (x, y). The solution procedure is briefly outlined below.

We begin with a guess solution: a parabolic velocity profile at every axial location, and march in psuedo-time until a steady-state solution is obtained. The governing equations are discritized using first-order accurate forward differencing in time and second-order accurate central differencing in space. The vorticity distribution at the new time step is calculated by solving the discritized unsteady vorticity equation using the velocity field in the previous time step. The streamfunction distribution is then calculated by solving the Poisson equation iteratively using a full-multigrid technique. It is to be noted here that our full-multigrid technique gives a speed-up of around 100 times as compared to the commonly used Jacobi iterative technique. From the updated values of streamfunction the velocity and vorticity at the walls are obtained. This procedure is repeated until the cumulative change in vorticity reduces to below 10^{-8}, which is consider as the criteria for the steady state. A grid of 514×144 is used in the x and y directions, respectively. Contours of components of the streamwise and the transverse velocity are given in figure 3 for $Re = 5$. As can be

discerned, the flow in this case is close to separation at the location where the turn from diverging to converging occurs. With an increase in the Reynolds number, a clearly defined separation zone appears, and a further increase in Re causes an increase in the length of the separation zone, as shown in the figure 4. For Reynolds number equals to 20 it can be seen in figure 4 that the flow becomes slightly asymmetric, resulting different size of separation bubble near the top and bottom walls.

The base flow has been obtained on a uniform grid, whereas for the disturbance (stability analysis discussed in the next section), the linearized Navier-Stokes equations are solved on a grid consisting of Chebyshev collocation points. The has been done as the linear stability analysis is very sensitive to the number of grids near the walls, where the viscosity effects are predominant. Thus, the resultant solution of the base flow is interpolated onto the spectral grid using an arc-length based cubic spline interpolation. These methods are specially designed to eliminate any spurious interpolation-induced oscillations.

2.2 Global Linear Stability Analysis

We conducted a two-dimensional global linear stability of the base flow obtained by solving equations (1)-(3) using a normal mode in time. Following the validity of the Squire's theorem in shear flows [32], we therefore restrict ourselves to two-dimensional perturbations. In the standard approach the flow variables are split into base state quantities (denoted by upper case letters) and two-dimensional perturbations (designated by hat), as

$$u = U + \hat{u}; \qquad v = V + \hat{v}; \qquad p = P + \hat{p} \tag{5}$$

Here, $\hat{u}(\equiv \partial\hat{\phi}/\partial y)$ and $\hat{v}(\equiv -\partial\hat{\phi}/\partial x)$ are the disturbance velocities in the streamwise and transverse, directions, respectively, and p is the disturbance pressure. $\hat{\phi}$ is the disturbance streamfunction. Expressing the time dependence in normal mode form as, $\hat{\phi}(x,y,t) = \phi(x,y)e^{-i\omega t}$, substituting the above in the momentum equations, linearising and eliminating pressure, we obtain

$$\left\{\left[U\frac{\partial}{\partial x} + V\frac{\partial}{\partial y}\right]\nabla^2 + \left[\frac{\partial^2 V}{\partial x \partial y} - \frac{\partial^2 U}{\partial y^2}\right]\frac{\partial}{\partial x}\right. \tag{6}$$
$$\left. + \left[\frac{\partial^2 U}{\partial x \partial y} - \frac{\partial^2 V}{\partial x^2}\right]\frac{\partial}{\partial y} - \frac{1}{Re}\nabla^4\right\}\phi = i\omega\nabla^2\phi,$$

which governs the evolution of disturbances in the flow. Here $i = \sqrt{-1}$, ω is the complex eigenvalue, whose real and imaginary parts give the frequency and the temporal growth rate of the disturbance, respectively. Note that a given mode is unstable if $\omega_i > 0$, stable if $\omega_i < 0$ and neutrally stable if $\omega_i = 0$.

In the present study the Reynolds number is low, and the geometry is strongly varying in the streamwise direction. Hence a global stability study, where the base flow and the amplitude of the perturbations are functions of both the streamwise (x) and transverse(y) co-ordinates, is appropriate, as opposed to a parallel study which considers homogeneity in the streamwise direction. A detailed report on global stability analysis is available in Theofilis [34]. This approach has been used to study various non-parallel flows, including separated flows [35], boundary layers [36, **?**,**?**], ducts [37], and solid rocket motors [38]. In a rectangular duct [39] reduced the global stability system to a single equation for the purpose of numerical simplicity. We follow a similar approach; both the base flow and the perturbations essentially consider homogeneity in the spanwise (z) direction.

2.2.1 Numerical Method

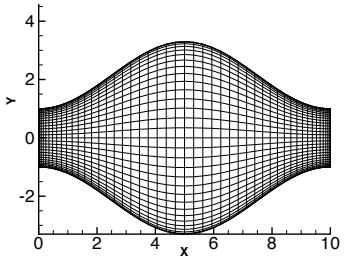

Fig. 5 A typical grid used for the global stability study; grid size is 51×31.

For easy satisfaction of the boundary conditions, the global stability equation (6) is expressed in the ζ-η (computational) plane. As explained earlier, for a global stability problem with perturbation amplitude being a function of both streamwise (x) and transverse (y) directions, the equation is discretized according to the Chebyshev spectral collocation technique in both spatial directions, with n points in the ζ direction and m points in the η direction. The two-dimensional discretization matrices are obtained appropriately by Kronecker product [34] in ζ-η coordinates.

In the transverse direction, it is desirable to have clustering (more grid points) close to the wall, and near the inlet and outlet of the channel where the gradients of velocity are the highest. This comes out naturally using Chebyshev spectral discretization. A typical grid on a geometry is shown in figure 5 for

$\epsilon = 2.3$ and $L = 10$. The equation in the discretized form results in a dense matrix which is solved using the LAPACK library. The maximum grid size used is 81×81, which gives the leading dimension of the matrix. However, as the typical critical Reynolds numbers are low, a resolution of 51×51 is sufficient to obtain the entire eigenspectrum accurately.

2.2.2 Boundary Conditions

The global stability equation 7 is solved using no-slip and no-penetration boundary conditions at the channel walls and periodic boundary conditions at the inlet and outlet of the channel, which are given by:

$$\phi_i = \phi_o \tag{7}$$

$$\left(\frac{\partial \phi}{\partial \zeta}\right)_i = \left(\frac{\partial \phi}{\partial \zeta}\right)_o \tag{8}$$

$$\left(\frac{\partial^2 \phi}{\partial \zeta^2}\right)_i = \left(\frac{\partial^2 \phi}{\partial \zeta^2}\right)_o \tag{9}$$

$$\left(\frac{\partial^3 \phi}{\partial \zeta^3}\right)_i = \left(\frac{\partial^3 \phi}{\partial \zeta^3}\right)_o \tag{10}$$

The subscript i and o indicate inlet and outlet of the channel, respectively for the stability grid.

3 Results

3.1 Validation

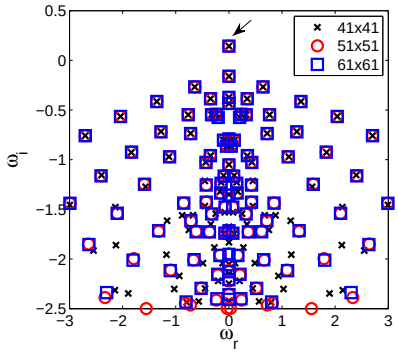

Fig. 6 Eigenspectra for flow through a converging-diverging channel with $\epsilon = 2.3$ and $L = 10$. Grid independence is shown using the stability grids ($n \times m$, n and m being the resolution in x and y direction respectively) as shown in the legend for $Re = 20$ (unstable case).

The numerical approach is first checked on a straight channel and found to yield the text-book Re_{cr} of 5772 for global stability as well. The length of the channel was prescribed as $L = 2\pi/1.02$, the known wavelength of the neutral mode at this Reynolds number.

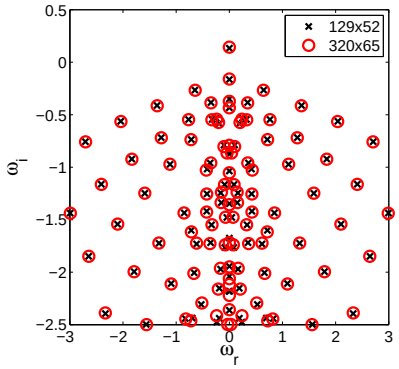

Fig. 7 Eigenspectra for flow through a converging-diverging channel with $\epsilon = 2.3$ and $L = 10$. Grid independence is shown using the mean flow grids ($n \times m$, n and m being the resolution in x and y direction respectively) as shown in the legend for $Re = 20$ for a stability grid of size 51×51. This is an unstable case, where grid insensitivity is usually harder to obtain.

In the converging-diverging case, the eigenspectrum obtained for the flow in a channel with $\epsilon = 2.3$ (highest aspect ratio considered) and $L = 10$ for $Re = 20$ is shown in figure 6. The grid size of the base flow used for this case is 320×65. We will discuss the physics pertaining to this result in the following subsection, but note here that grid convergence is excellent. It has been checked that the results are equally insensitive to the grid on which the mean flow is obtained, and example is given in the figure 7. It can be seen that 51×51 is enough to obtain accurately the entire top half of the eigenspectrum even for $Re = 20$, which is the highest Reynolds number considered in the present stability analysis. The best resolutions shown here are used in the rest of this study for stability calculations.

3.2 Results: Global Linear Stability

Figure 6 shows that the flow through our standard geometry is unstable at a Reynolds number of 20. The instability appears with a single mode seen to go unstable, i.e., with a positive growth rate, ω_i. It is seen that this is a stationary mode, i.e., with a circular frequency $\omega_r = 0$. We note that at higher Reynolds numbers and smaller ϵ it is usually a traveling mode that becomes unstable first. We note also that the growth rate of $\omega_i = 0.1431003$ is high, it is enough to double the amplitude of the disturbance in less than 5 time units. In a plane channel, even at a Reynolds number of 6000, the leading eigenmode grows orders of magnitude slower. The leading mode (marked by the arrow in figure 6) is visualized in figure 8, where the top, middle and bottom panels respectively show the real

parts of the disturbance streamfunction, and the disturbance velocity components in the streamwise and transverse directions. All three figures demonstrate that this is a symmetry-breaking mode, with parcels of fluid executing anti-clockwise motion relative to the base flow.

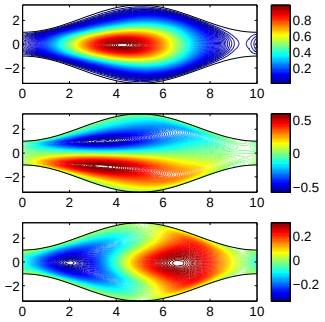

Fig. 8 The real part of the streamfunction ϕ (top), streamwise velocity, u (middle) and the transverse, v (bottom) of the leading (unstable and stationary) mode. [The imaginary parts of the components are equal to 0.]

The eigenspectra obtained from the global stability analysis using 51×51 for a flow in a converging-diverging channel with $\epsilon = 2.3$ for $Re = 10$ is shown in figure 9. It can be seen that the mode (marked 1) lies above the dashed line, $\omega_i = 0$, indicating that the flow is unstable. A comparison with figure 6 reveals that the growth rate of the most unstable mode for $Re = 10$ is less than that for $Re = 20$. Figure 10 shows eigenfunctions of the different typical modes form the least stable branch of the eigenspectrum shown in figure 9. Modes 1 and 2 with the least stable ω_i are stationary or purely growing/decaying without any frequency of oscillation (thus only real part of the disturbance streamfunctions is shown) while modes 3, 7 and 15 are travelling modes with a finite frequency of oscillation. The real and imaginary parts of the streamwise velocity components are shown in this plot. Close inspection also revels that the modes are not wave-like and the amplitude functions themselves depend on both x and y.

In order to investigate the effects of Reynolds number the upper branch eigenspectra are plotted for four different values of Re in figure 11. Figure 12 shows the real part of the disturbance streamwise velocity of leading mode for the stable case, $Re = 5$ (top) and the unstable case, $Re = 20$ (bottom). It is seen that with an increase in the value of Re the least stable branches start moving upwards thus becoming more unstable. The structures of the leading modes obtained for the

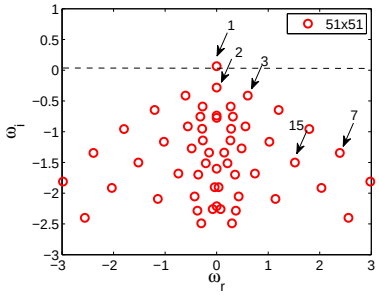

Fig. 9 Eigenspectrum for the flow in a converging-diverging channel with $\epsilon = 2.3$ and $L = 10$ for $Re = 10$ (unstable case) and resolution shown in the legend. [Periodic boundary condition is imposed at the inlet and outlet]

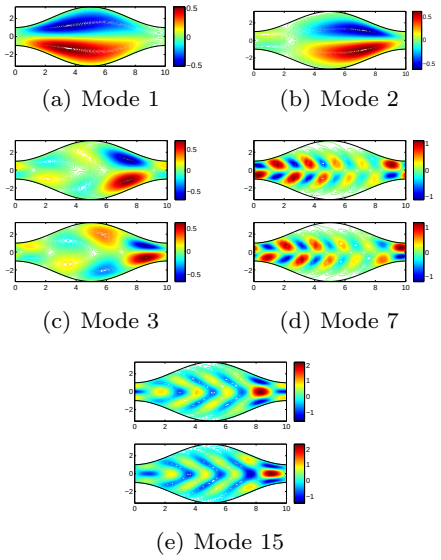

Fig. 10 Perturbations (real/imaginary parts of the streamwise velocity component, u) marked by the arrows in Figure 9. (a-b) The real parts of u for the stationary modes (c-e). The real (top) and imaginary (bottom) parts of u for the travelling modes.

different values of Re are similar to each other, with a slight elongation at the inlet for $Re = 20$.

In Figure 13, we plot the maximum growth rate of the least stable (leading) mode as a function of Reynolds number for different values of ϵ. It is seen that the critical Reynolds number decreases though not very significantly with an increase in the amplitude of wall-waviness, ϵ. We found that the critical Reynolds for $\epsilon = 2.3$ is around 8. A further increase in ϵ does not decrease the critical Reynolds number significantly. The critical Reynolds numbers were seen earlier in figure 2, where the decrease of this quantity with an increase in angle is seen to slow down. Incidentally a Reynolds number of 10 corresponds to the flow of water at 1 centimeter per second through a 1 millimeter wide channel.

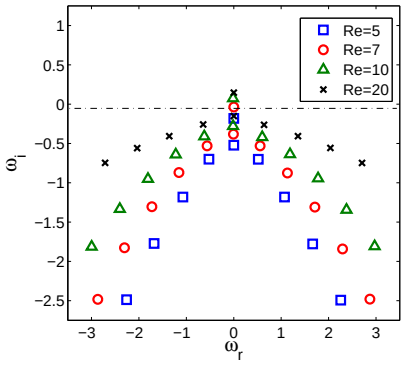

Fig. 11 The least stable branch of eigenspectra and the leading eigenmode for the different Re.

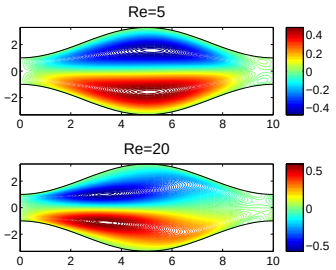

Fig. 12 The real part of the streamwise velocity (u) of the leading eigenmode for $Re = 5$ (top) and $Re = 20$ (bottom).

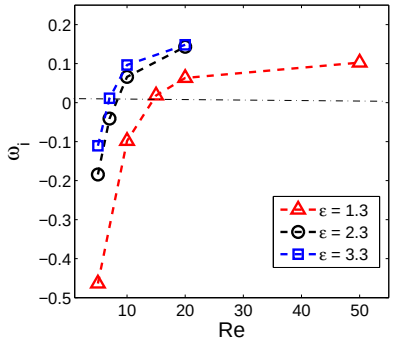

Fig. 13 Converging-diverging channel with $L = 10$ for different ϵ, maximum amplitude of wall-waviness to minimum half-width of the channel. The growth rate, ω_i of the least stable eigenmode as a function of the Reynolds number is shown. The flow is neutrally stable at $\omega_i = 0$, which defines the critical Reynolds number.

4 Conclusion

A global linear stability analysis has been carried out for sinusoidally varying periodic channels. The critical Reynolds number is obtained for different wall-waviness amplitude. It is shown that with an increase in the amplitude of the wall-waviness the critical Reynolds number reduces by a large amount. At these low Reynolds numbers, we find a leading mode that grows exponentially in time while remaining stationary in space, whereas an oscillatory flow has been observed by others at higher Re. The standing mode contains closed streamlines relative to the mean flow, where flow circulates in an anti-clockwise sense when the flow is from left to right. The length scale of this leading mode is the same as that of the channel geometry. The eigenspectrum is shown to consist of several distinct branches which lean downwards in complex frequency space. The eigenstructure is similar at different Reynolds numbers in this range, with the least stable eigenmode always being a stationary one of similar modal structure. Structures of smaller typical length scales are displayed by the higher modes on the branches, and these are in the form of traveling waves. Algebraic growth of instabilities and nonlinear interactions among stationary and traveling modes may lead to enhanced mixing, and these are suggested as future avenues to be explored. Releasing the periodic boundary condition in these nonlinear studies may lead to richer dynamics.

References

1. A. McAlpine, P.G. Drazin, Fluid Dynamics Research **22**, 123 (1998)
2. G. Swaminathan, A. Sameen, K.C. Sahu, R. Govindarajan, Theoretical and Computational Fluid Dynamics **25**, 53 (2011)
3. J. Peixinho, H. Besnard, Physics of Fluids **25**, 111702 (2013)
4. V. Duryodhan, S. Singh, A. Agarwal, Microfluid Nanofluid **14**, 53 (2013)
5. S. Tripathi, A. Prabhakar, N. Kumar, S.G. Singh, A. Agrawal, Biomedical microdevices **15(3)**, 415 (2013)
6. I.J. Sobey, J. Fluid Mech. **96**, 1 (1980)
7. K.D. Stephanoff, I.J. Sobey, B.J. Bellhouse, J. Fluid Mech. **96**, 27 (1980)
8. T. Nishimura, Y. Ohori, Y. Kawamura, J. of Chemical Engineering of Japan **17, 5**, 466 (1984)
9. S. Blancher, R. Creff, J. Batina, P. Andre, Finite Elements Analysis and Design **16**, 261 (1994)
10. K.J. Cho, M. Kim, H.D. Shin, Fluid Dynamics Research **23**, 349 (1998)
11. T.A. Rush, T.A. Newell, A.M. Jacobi, International Journal of Heat and Mass Transfer **42**, 1541 (1999)
12. S. Selvarajan, E.G. Tulapurkara, V.V. Ram, Phys. Fluids **11, 3**, 579 (1999)
13. K. Stone, S. Vanka, Journal of Fluids Engineering **121**, 713 (1999)
14. J.M. Floryan, J. Fluid Mech. **482**, 17 (2003)
15. P.M. Eagles, Journal of Fluid Mechanics **24, part 1**, 191 (1966)
16. K.C. Sahu, R. Govindarajan, Journal of Fluid Mechanics **531**, 325 (2005)
17. K.C. Sahu, Proceedings of the Sixth IUTAM Symposium on Laminar-Turbulent Transition, Bangalore, India (2004)
18. S. Blancher, R. Creff, Phys. Fluids **16, (10)**, 3726 (2004)
19. S.K. Kim, Proceedings of the Sixth Asian Symposium on Visualization, Pusan, Korea pp. 349–370 (2001)

20. A.M. Guzman, C.H. Amon, Phys. Fluids **6, (6)** (1994)
21. A. Cabal, J. Szumbarski, J.M. Floryan, J. Fluid Mech. **457**, 191 (2002)
22. J.M. Floryan, Phys. Fluids **17, 044101**, 1 (2005)
23. J.M. Floryan, European Journal of Mechanics B/Fluids **26**, 305 (2007)
24. J.M. Floryan, C. Floryan, Fluid Dyn. Res. **42,2**, 025509 (2010)
25. J. Floryan, M. Asai, Physics of Fluids **23**, 104101 (2011)
26. J. Szumbarski, J.M. Floryan, J. Fluid Mech. **568**, 243 (2006)
27. J.P. Laval, M. Marquillie, Progress in Wall Turbulence: Understanding and Modeling, ERCOFTAC Series **14**, 203 (2011)
28. M. Akbari, D. Sinton, M. Bahrami, International Journal of Heat and Mass Transfer pp. 3970–3978 (2011)
29. B.M. Jose, T. Cubaud, Microfluid Nanofluid **12**, 687 (2012)
30. J. Peixinho, Seventh IUTAM Symposium on Laminar-Turbulent Transition (2010)
31. C. Amon, A.M. Guzman, B. Morel, Phys. Fluids **8**, 1192 (1996)
32. P.G. Drazin, W.H. Reid, Cambridge University Press (1981)
33. T.N. Venkatesh, V.R. Sarasamma, S. Rajalakshmy, K.C. Sahu, R. Govindarajan, Current Science **88(4)**, 589 (2006)
34. V. Theofilis, Progress in Aerospace Sciences **39**, 249 (2003)
35. V. Theofilis, S.J. Sherwin, N. Abdessemed, NATO RTO-AVT **RTO-AVT-111**, 21 (2004)
36. V. Theofilis, A. Federov, D. Obrist, U.C. Dallmann, Journal of Fluid Mechanics **487**, 271 (2003)
37. V. Theofilis, P.W. Duck, J. Owen, Journal of Fluid Mechanics **505**, 249 (2004)
38. F. Chedevergne, G. Casalis, T. Feraille, Phys. Fluids **18**, 014103 (2006)
39. T. Tatsumi, T. Yoshimura, Journal of Fluid Mechanics **212**, 437 (1990)